AIAA JOURNAL
Vol. 45, No. 12, December 2007

Implementation of a Phased Microphone Array in a Closed-Section Wind Tunnel

H.-C. Shin* and W. R. Graham†
University of Cambridge, Cambridge, England CB2 1PZ, United Kingdom
P. Sijtsma‡
National Aerospace Laboratory/NLR, 8300 AD Emmeloord, The Netherlands.
and
C. Andreou§ and A. C. Faszer§
University of Cambridge, Cambridge, England CB2 1PZ, United Kingdom

DOI: 10.2514/1.30378

This paper describes the design and implementation of a phased microphone array system for aeroacoustic measurements in a closed-section wind tunnel at the Department of Engineering at the University of Cambridge. The tunnel has a test-section area of 1.67 × 1.22 m and can generate wind flows up to 60 m/s. The research started by conducting a feasibility study to find out whether an array could be used in the presence of the tunnel background noise. The boundary-layer pressure fluctuations were found to be correlated according to the Corcos model (Corcos, G. M., *Journal of Fluid Mechanics*, Vol. 18, No. 3, 1964, pp. 353–378.). Their level can be reduced by recessing microphones away from the flow, but the benefits of such an approach in this facility were found to be insufficient for it to be followed. Two different size arrays, for frequency ranges 650 ∼ 6500 Hz and 5 ∼ 50 kHz, were designed and installed. A range of characterization and shakedown experiments are described; in particular, it is shown that averaging can increase signal-to-noise ratio and that the array can detect sources up to 6 dB below the mean cross-spectral level of the background noise.

Nomenclature

i	=	imaginary unit of $\sqrt{-1}$
p	=	pressure fluctuation
r_x	=	streamwise separation in the Cartesian coordinate
r_y	=	tunnel spanwise separation in the Cartesian coordinate
U_c	=	boundary-layer eddy convection velocity
V	=	freestream speed inside the wind tunnel
x	=	streamwise direction
y	=	tunnel spanwise direction
α_x	=	streamwise attenuation rate
α_y	=	tunnel spanwise attenuation rate
Δf	=	frequency bandwidth
Δx	=	streamwise spacing for the cross-spectra microphone pair
Δy	=	tunnel spanwise spacing for the cross-spectra microphone pair
ρ	=	density of air
$\Phi(\omega)$	=	boundary-layer pressure spectrum at the angular frequency of ω
ω	=	angular frequency

Presented as Paper 2651 at the 12th AIAA/CEAS Aeroacoustics Conference, Cambridge, MA, 8–10 May 2006; received 11 February 2007; revision received 7 August 2007; accepted for publication 8 August 2007. Copyright © 2007 by the authors. Published by the American Institute of Aeronautics and Astronautics, Inc., with permission. Copies of this paper may be made for personal or internal use, on condition that the copier pay the $10.00 per-copy fee to the Copyright Clearance Center, Inc., 222 Rosewood Drive, Danvers, MA 01923; include the code 0001-1452/07 $10.00 in correspondence with the CCC.

*Research Associate, Department of Engineering. Member AIAA.
†Senior Lecturer, Department of Engineering. Member AIAA.
‡Senior Scientist, Department of Helicopters & Aeroacoustics, P.O. Box 153.
§Ph.D. Research Student, Department of Engineering. Student Member AIAA.

I. Introduction

THIS paper describes the design and implementation of a phased microphone array system in the Markham closed-section wind tunnel at the Department of Engineering at the University of Cambridge. The tunnel has a test-section area of 1.67 m (width) × 1.22 m (height) and can generate wind flows up to 60 m/s.

Wind tunnels have been traditionally used for the aerodynamic evaluation of test models and only recently for aeroacoustic experiments. The extra challenge encountered for aeroacoustic applications is that the background-noise level may be too high to detect a genuine noise from a test model. In this aspect, two separate approaches have been taken to overcome such a low signal-to-noise ratio problem. Each method has been favored initially by one of two important industries. The automotive industry has invested heavily in building acoustic wind tunnels with a low background-noise level, whereas the aerospace industry has developed advanced acoustic measurement technologies, which effectively increase signal-to-noise ratio in a postprocessing stage [1]. For each industry, the other approach had been usually a secondary priority, although recently both sides have started to adopt the other option.

A possible reason for the industries favoring different methods is that the automotive industry usually conducts both interior and exterior acoustic measurements, for up to a full-scale vehicle, in relatively low flow speeds, whereas the aerospace industry carries out mostly exterior acoustic measurements, for a scaled-down model or a full-size component, in relatively high flow speeds. Modern automotive facilities are, however, capable of relatively high wind speed, matching that of aerospace wind tunnels. Unlike an exterior experiment, in an interior measurement, the number of microphones is restricted, and hence the need for a quiet wind tunnel has been paramount in the automotive industry. Meanwhile, in the aerospace industry, because the size and flow speed of wind tunnels are more demanding than those of the automotive industry, advanced acoustic measurement technologies (e.g., incorporating multiple microphones) are a reasonable option. Also, considering that exterior measurements tend to search for a location of acoustic sources, whereas interior measurements focus more on the quality of interior sound, the investment in advanced technologies has been inevitable for exterior acoustic measurements. Among these new technologies,

a phased microphone array and associated beam forming, which has been borrowed from other branches of science and engineering such as astronomy, underwater acoustics, etc., has been extensively adopted for the aeroacoustic measurements in wind tunnels [2–10]. In addition, the availability and accessibility of such a system has been made easier in the last decade, due to innovation in the equipment manufacturing industry.

The Markham wind tunnel has been used predominantly for the aerodynamic evaluation of test models and has no acoustic treatment. The array is required for experimental research into the current main sources of airframe noise: high-lift devices and landing gear. Array systems are, however, now recognized as capable of providing the required measurements in closed-section wind tunnels that have had no special acoustic treatment. Because the installation of a microphone into an existing tunnel is relatively straightforward compared with acoustic treatment (or the development of a new facility), this was the approach taken.

The following sections are Feasibility Study, Equipment, Array Design and Manufacture, Effect of Averaging on the Cross Spectra, Array Measurement and Beam Forming, and Conclusions. The feasibility study considers the background-noise characteristics of the Markham wind tunnel and their implications regarding the microphone type and mounting scheme. In the next section, the instrumentation used in the array system is briefly discussed. Then the key performance characteristics of the arrays that were implemented are presented. In practice, measurement quality is dependent on signal-to-noise ratio, and the cross-spectral properties of all microphone pairs in the installed arrays are therefore considered to address this question. Finally, the beam-forming results for some initial shakedown tests to evaluate the capability of the array system are reported.

Much of the discussion in the paper concerns spectral quantities, either the (purely real) autospectra of single microphone signals or the (complex) cross spectra between microphone pairs.¶ The latter are presented as amplitude and phase components, referred to as cross spectra and phase angle, respectively. When spectra are referenced to a constant bandwidth (also known as a narrowband analysis), the amplitude levels are expressed in pressure spectrum level, rather than sound pressure level. This convention is useful because a direct comparison is made possible between results with different frequency bandwidths. Also, information on bandwidth is provided, if necessary. The pressure spectrum level [11] (also sound pressure spectrum level [12]) is defined as $10\log_{10}\{(p^2/\Delta f)/(p_0^2/\Delta_0 f)\}$ decibels (dB), where p^2 is the time-mean-square sound pressure of a specified frequency band, Δf is the bandwidth, p_0 is the reference sound pressure of 20 μPa, and $\Delta_0 f$ the reference bandwidth of 1 Hz. Alternatively, a spectrum may be presented in the $\frac{1}{3}$-octave bandwidth of a constant percentage bandwidth. In this case, the amplitude is expressed as a sound pressure level, following the widely accepted convention. The phase angles are displayed in degrees.

II. Feasibility Study

A. Microphone Flow-Induced Noise

For inflow use of microphones, it is recommended that protection grids on top of microphone cartridges be removed [8]. This, however, exposes the fragile diaphragm of the microphones to the risk of damage. One suggestion is to mount microphones after experiment setup, but this may not always be practical. The reason for removing protection grids is to avoid extraneous noise generated due to their nonuniform surface [8]. However, because such removal poses practical difficulties, it is worth investigating the microphone flow-induced noise associated with grids.

Two types of microphone were tested. The first, Brüel and Kjær (B&K) model 4135, is a $\frac{1}{4}$-in. precision condenser microphone with a protection grid. The other, LinearX Systems model M51, has an outer diameter of $\frac{1}{2}$ in. but a smaller diaphragm, approximately 2 mm in diameter, which is exposed rather than covered by a protection grid. At a flow speed of 60 m/s (Fig. 1a), the B&K microphone signal is significantly higher than that of the LinearX in both auto- and cross spectra. At the lower speed of 20 m/s (Fig. 1b), the discrepancy is significantly reduced. These results demonstrate that protection grids are prone to generate extraneous flow-induced noise, for which the contribution increases with flow speed.

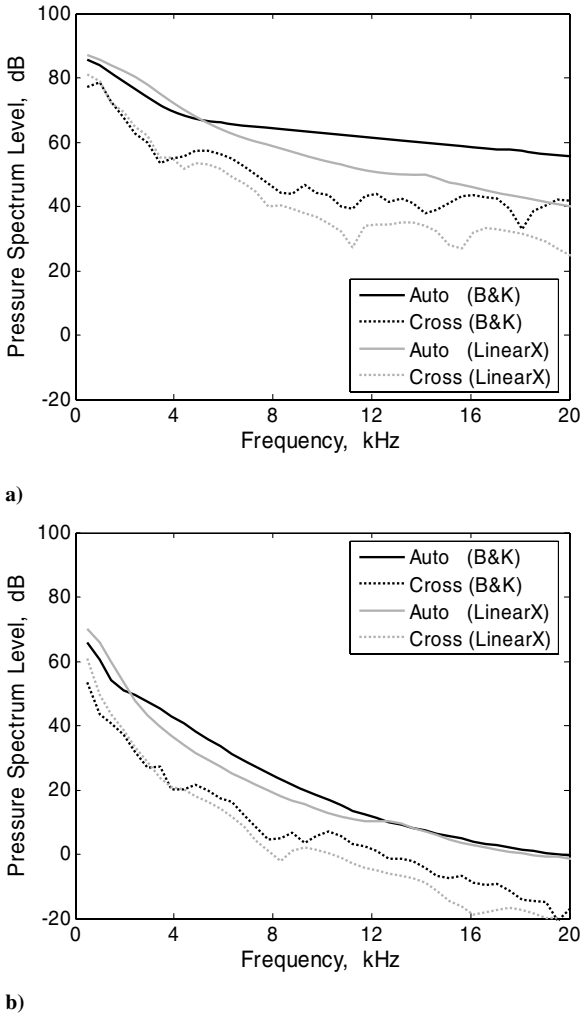

Fig. 1 Auto- and cross-spectral measurements of background-noise level by two different types of microphones for a) 60 m/s freestream speed and b) 20 m/s freestream speed. The B&K model is a $\frac{1}{4}$-in. condenser microphone with a protection grid on. The LinearX model is a microphone with an exposed diagram of approximately 2 mm in diameter. Microphone spacing for cross spectra is 4 cm streamwise.

Based on these findings, the LinearX microphones were specified for subsequent measurements. Although not perfectly protected, they are believed to pose less risk than larger diaphragm microphones with grids removed.

B. Background-Noise Level

Background-noise measurements in the empty wind tunnel were conducted with a few microphones flush-mounted on the tunnel floor. The results showed that both fan noise and turbulent boundary-layer pressure fluctuations were significant components. Fan tones at blade-passing frequency and its harmonics were clearly identifiable up to around 650 Hz, depending on the tunnel speed.

Above 650 Hz, due to the less coherent characteristics of the boundary-layer pressures, the cross spectra of pairs of microphones were significantly reduced from their autospectra (see Fig. 1). As is

¶The signals for which the spectra are being displayed are microphone signals generated by aeroacoustic sources and background noise in the wind tunnel, and the cross spectra are evaluated between various pairs of microphone signals observing the same events from different locations.

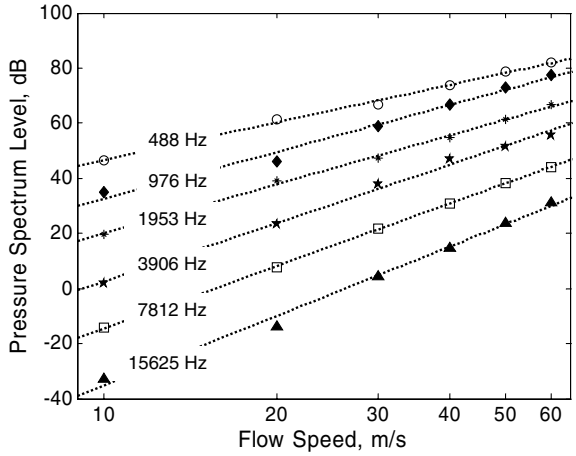

Fig. 2 Power-law dependence of background-noise cross spectrum. Discrete marks are measurements and associated lines of regression represent the power-law relationships: $p^2 \sim V^{4.5}$ (488 Hz), $p^2 \sim V^{5.7}$ (976 Hz), $p^2 \sim V^{5.9}$ (1953 Hz), $p^2 \sim V^{7.1}$ (3906 Hz), $p^2 \sim V^{7.5}$ (7812 Hz), and $p^2 \sim V^{8.4}$ (15,625 Hz), respectively. Analysis bandwidth is 488 Hz and microphone spacing is 2.8 cm.

well known [13], this is a key factor that makes a phased microphone array system feasible under the significant background-noise levels inside a closed test-section wind tunnel. Also as expected, auto- and cross spectra showed a strong dependence on the flow speed. The results for cross spectra are shown in Fig. 2, along with the best-fit power-law relationships $p^2 \sim V^{4.5}$ (488 Hz), $p^2 \sim V^{5.7}$ (976 Hz), $p^2 \sim V^{5.9}$ (1953 Hz), $p^2 \sim V^{7.1}$ (3906 Hz), $p^2 \sim V^{7.5}$ (7812 Hz), and $p^2 \sim V^{8.4}$ (15,625 Hz). They suggest that the sound pressure scales at low frequencies with the dynamic pressure characterized by $0.5\rho V^2$ and at high frequencies with turbulence-generated pressure fluctuations that are proportional to V^4. The power-law coefficients were found to vary slightly from channel to channel, but with standard deviations below 4% of their mean values.

C. Recession of Microphones

Underbrink [8] recommends that microphones are mounted as flush as possible to minimize flow noise caused by either recess or protrusion. Flush microphones are believed to experience less turbulence than protruded microphones and to be free from vortex-shedding tones at the cavity edge of a recess. Contrary to the adverse effect of individual microphone recession, however, a benefit has been reported when a panel of microphones is set back from a tunnel wall and separated from the flow [5]. One might also expect recession to be beneficial in reducing the microphone flow-induced noise associated with a protection grid. The effect of microphone recession was therefore investigated during the feasibility study.

First, individual recession to reduce microphone flow-induced noise was tested. Recessing microphones individually has been reported to alter their frequency and directional response [14]. Here, however, we focus on the change in the sound level with recession distance. When B&K microphones were recessed 2 and 5 mm from the tunnel floor, their flow-induced noise was found to be reduced, but was still higher than or, at best, similar to that of flush-mounted LinearX devices. Second, a small section of the floor was recessed with a cover of either fine metal mesh or Kevlar® cloth, introduced to keep the turbulent flow away but to allow acoustic signals to reach the microphones. This configuration is expected to eliminate the contribution to the background noise of the boundary-layer pressure fluctuations, which are predicted to decay exponentially with recession depth [5]. Recessions of 10 and 20 mm were tested. Figure 3a shows how the LinearX microphone autospectra are affected by the various recession schemes at the speed of 30 m/s. The evanescent characteristics of the boundary-layer pressure fluctuations are observed up to 10-mm recession, depending on frequency. However, no significant extra benefit is gained by increasing the depth from 10 to 20 mm, suggesting that the boundary

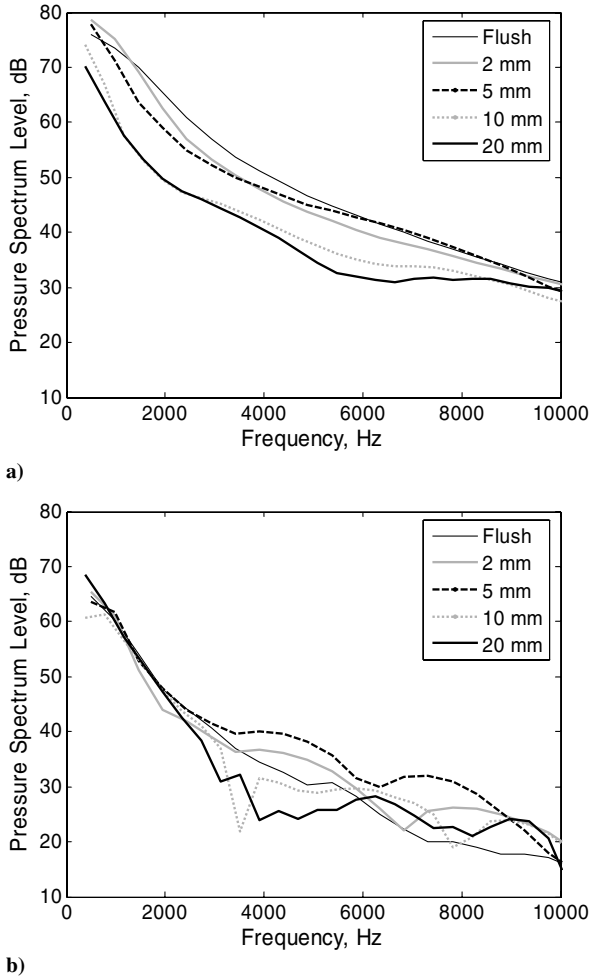

Fig. 3 Effect on a) autospectra and b) cross spectra by different recession depths at 30 m/s. LinearX microphones were individually recessed to the depth of 2 and 5 mm. The plate of LinearX microphones was recessed to the depth of 10 and 20 mm, and the cavity was covered by a fine metal mesh. The bandwidth for flush mounting and individual recession is 488 Hz and the other is 391 Hz. Microphones for the cross spectra were separated by 4 cm along the streamwise direction.

layer is no longer the dominant source. Figure 3b shows the corresponding cross spectra. Unlike the autospectra, there is almost no difference below 3000 Hz. Note also that the cross-spectrum levels of the 10- and 20-mm recessions match those of the autospectra, confirming the elimination of the boundary-layer pressure contribution in the latter cases. At higher frequencies (above around 3000 Hz), the cross spectra seem to experience modulation based on microphone spacing. Whether a recession scheme is necessary for the array design is discussed in Sec. II.D.

The narrower bandwidth analysis shown in Fig. 4 also implies a noise source other than the boundary-layer pressure. The tonal peaks are generated by the wind-tunnel fan. The 27.4-Hz frequency is close to the blade-passing frequency of 26.3 Hz for four blades at 395 rpm. The other distinct tonal components are close to the harmonics of 27.4 Hz. Both the tones and the broadband noise components are well-correlated, as shown by the almost identical levels of the auto- and cross spectra. This implies no significant reduction of background noise at these frequencies through the cross-spectral evaluation implemented in a beam-forming process.

At this stage, it is worth noting that there are mainly two different mechanisms for background noise recorded by microphones on the flush mounting. One has an acoustic nature generated by the interaction between the flow and the wind-tunnel structure, such as a fan and a guide vane. The other is caused by hydrodynamic pressure fluctuations present in the turbulent boundary layer along the tunnel surface.

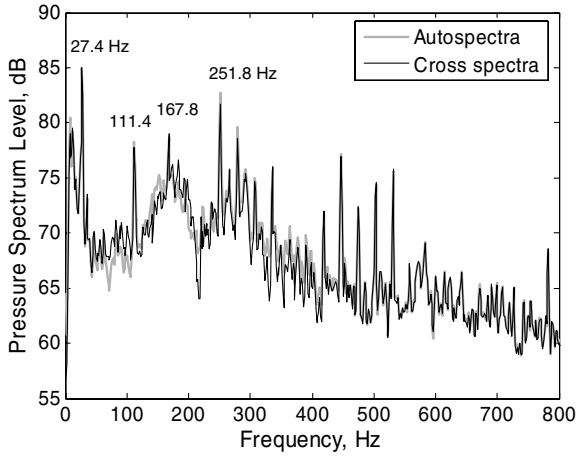

Fig. 4 Effect on the auto- and cross spectra by the recession of microphones and tonal noise components at 30 m/s. The bandwidth is 1.5 Hz. A plate of microphones was recessed by 20 mm, and its entry was covered by a fine wire mesh.

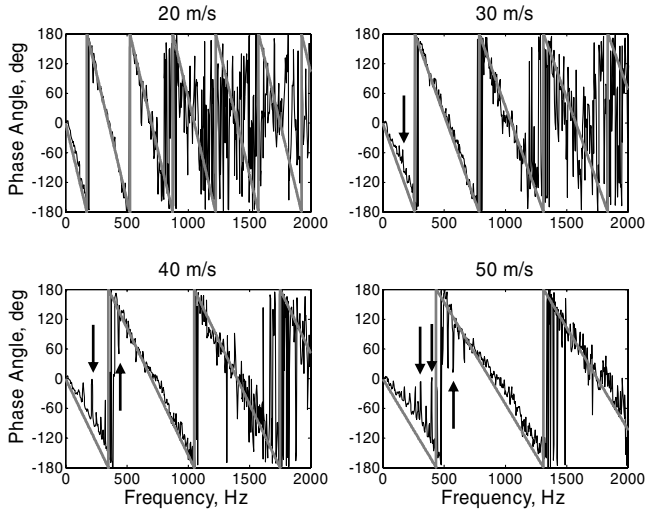

Fig. 5 Application of the Corcos model to the phase information of a microphone pair. The noisy black line is the measured phase variation, and the smooth gray line is the Corcos model with a convection speed of 70% freestream speed. The bandwidth is 3.8 Hz. Microphones are separated 4 cm apart streamwise.

D. Corcos Model

Corcos [15] proposed an empirical model for the spatial correlation between surface pressures in boundary-layer flows. The cross spectrum $\Phi_p(r_x, r_y, \omega)$ of boundary-layer pressures separated by x and y components r_x and r_y is related to their autospectrum $\Phi(\omega)$ by

$$\Phi_p(r_x, r_y, \omega) = \Phi(\omega) \exp(-\alpha_x|\omega r_x|/U_c) \exp(-\alpha_y|\omega r_y|/U_c) \exp(i\omega r_x/U_c) \tag{1}$$

where U_c is the boundary-layer eddy convection velocity, which is typically 70% of a mainstream speed. Various values for the constants α_x and α_y are given in the literature; here, $\alpha_y = 0.7$ and $\alpha_x = 0.116$ are used [16].

Figure 5 shows the cross-correlation phase for a microphone pair separated by 4 cm streamwise and the prediction from Eq. (1). The agreement is excellent at lower frequencies and extends over a greater range as the flow speed increases, implying that the turbulent boundary layer gets more significant. An interesting aspect is the departure from the Corcos model at frequencies in which there is a dominant noise from another source. An example is fan tones, some

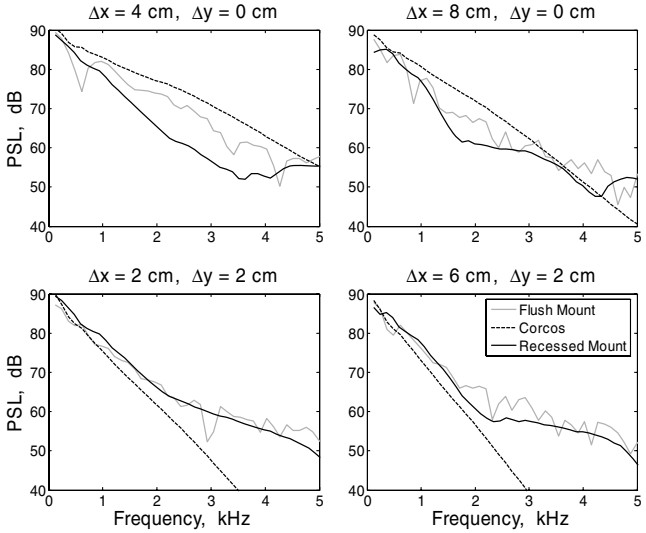

Fig. 6 Application of the Corcos model to the amplitude of cross spectra of four microphone pairs. Measured spectra are shown in solid lines, and the Corcos model is shown in dashed lines. The flow speed is 60 m/s; Δx and Δy indicate microphone separation along the streamwise and spanwise directions, respectively.

of which are indicated by vertical black arrows. This also confirms that the phase speed of fan tones is much faster than that of the turbulent boundary layer. A systematic deviation from the Corcos model over the first 180-deg phase variation indicates boundary-layer convection velocities greater than 70% of freestream at low frequencies.

Figure 6 compares the cross-spectrum amplitude of four microphone pairs with the Corcos model predictions for a flow speed of 60 m/s. Also shown are the corresponding measurements for the 20-mm recessed panel (Sec. II.C). The flush-mounted results are observed to follow the Corcos model reasonably well over the first 2 kHz. Furthermore, at this flow speed, there is a potentially useful reduction in cross spectrum associated with recession for the 4 cm streamwise separation. Little benefit is, however, seen for the other pairs. In addition, the cross-spectral decay with microphone spacing is observed, especially for the streamwise pairs of flushed microphones.

The significant boundary-layer component demonstrated here raises a query over the results of Sec. II.C, which showed similar cross-spectrum amplitudes for flush-mounted and recessed microphones (Fig. 3b). The latter are associated with well-correlated acoustic signals, which should also contribute to the flush-mounted amplitude. However, there is no evidence of their doing so. One possibility is that the recession scheme itself scatters hydrodynamic pressure fluctuations into acoustic components. Although this issue would bear further investigation, it was not pursued here, because the results of Fig. 6 show that boundary-layer contributions to the cross spectra will only be significant for streamwise-separated microphone pairs with spacing less than about 5 cm. In Sec. IV, it will be seen that the array designed for this frequency range has much greater microphone separations. Smaller values are found in the higher-frequency array design, but in this range, the Corcos model shows that the boundary-layer component lies well below the measured cross spectra. A recessed array design is thus unnecessary in our facility.

E. Experiment Measurability

The measured background noise was compared with published sound levels of items with high-lift devices: a 4.7% scale model of a DC-10 aircraft with flap and slat deployed [17], and conventional and circulation control wings with flaps [18]. Corrections were made for frequency bandwidth, hard-wall tunnel, distance from model to microphones, and Mach number. Figure 7 shows the corrected spectra and the background cross-spectrum amplitude for a pair of microphones 4 cm apart streamwise, demonstrating that the high-lift

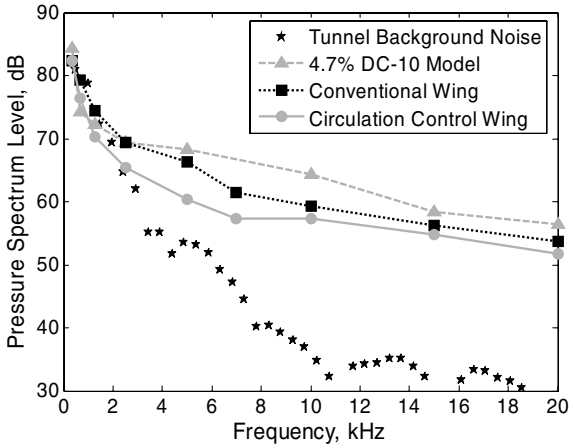

Fig. 7 Comparison between the Markham background-noise level and wing/aircraft model tests at 60 m/s.

devices noise levels would be measurable in the Markham wind tunnel. Given that the additional benefits of multichannel signal processing are not yet accounted for, it was concluded that a tunnel-based array could be used for the required measurements.

III. Equipment

A. Microphones

The LinearX Systems model M51 is a prepolarized condenser microphone. The mean and standard deviation of frequency responses of our 100 microphones are plotted in Fig. 8. For comparison, the frequency response of the B&K 4135 with a protection grid is also shown. Because the lower limit of array operation is around 650 Hz, the only significant difference is at high frequencies. This is compensated in the postprocessing stage, in which the frequency spectra of the raw signals are divided by the individual responses to remove microphone-to-microphone discrepancies. For response information above 40 kHz, extrapolation is used.

The nominal maximum sound level measurable by M51 microphones is 150 dB referenced to 20 μPa, and the minimum is 34 dB. The overall sound pressure level of our tunnel background noise varies from around 80 dB at 10 m/s up to 120 dB at 60 m/s. The nominal operating temperature is from 0 to 40°C. The exact tunnel temperature depends on its running speed, but is around 25°C. The microphones' temperature coefficient is -0.01 dB/°C, which ensures that the sound levels recorded at different speeds are comparable. The M51 requires a DC voltage supply of 10 V, which is provided by the data-acquisition system chosen, as discussed in the next section.

B. Signal Conditioning and Data Acquisition

A suitable combined signal-conditioning and data-acquisition unit is the GBM VIPER system [6]. It has built-in programmable gain amplifiers, anti-aliasing low-pass filters linked to sampling frequency, and high-pass filters selected at 1, 650, or 5000 Hz (chosen for the specific acoustics of our wind tunnel).** The channel count is 48, all of which are operated in simultaneous sample-and-hold continuous-acquisition mode. The maximum sampling rate available is 250 kHz per channel and the analog-to-digital converter resolution is 16 bits. Integrated power supplies for electret microphones (10 V) or pressure transducers (12 V) are included. In addition, a RAID system with a tape backup was installed to store the raw measurement data.

**The cutoff frequency of 650 Hz was determined based on the range of significant fan tonal noise (see Sec. II.B). Turbulent boundary-layer pressure was found to be dominant up to 5000 Hz (see Fig. 6). These frequencies also correspond to the lower end of nominal operating ranges in our arrays, as will be discussed in Sec. IV.

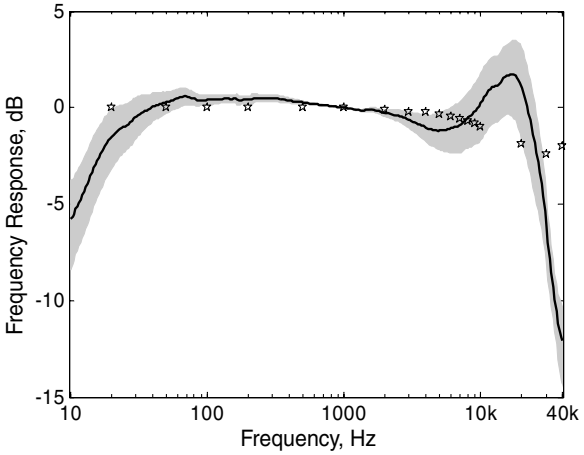

Fig. 8 Frequency response of microphones in the frequency range from 10 Hz to 40 kHz. The black line shows the mean of 100 LinearX M51 microphones. The gray area shows its standard deviation. These microphones are calibrated at 1000 Hz at the factory. The discrete pentagrams indicate the frequency response of a B&K 4135 microphone, which is calibrated at 250 Hz.

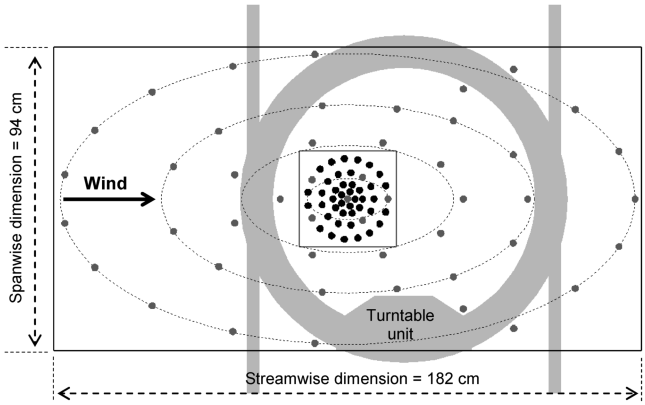

Fig. 9 Schematic diagram showing the geometry of both low- and high-frequency arrays. Microphones for the low-frequency array are shown as gray circles. Microphones for the high-frequency array are represented by black circles and gray circles inside the gray square. The microphone locations of the low-frequency array are modified from the ideal elliptic pattern, due to the presence of a turntable supporting unit and the aluminum plate holding the high-frequency array, which is represented by the gray square. Dimensions of all elements are in proportion. The streamwise direction is from left to right, as indicated by the arrow.

IV. Array Design and Manufacture

At the design stage, it was decided to have two 48-channel arrays, one for high-frequency and the other for low-frequency applications. There are two fundamental parameters that characterize the performance of an array: resolution and side-lobe level [19,20]. In this paper, the nominal resolution is defined as the width of the main lobe at 3 dB below its peak. For the high-frequency array, this parameter was selected to be 15 cm at its lower-end frequency of 5000 Hz when the focus is on a monopole source 60 cm overhead. This implies a resolution of approximately 2.2 times the corresponding acoustic wavelength at a given frequency. The array pattern consists of a number of concentric circles with a maximum diameter of 25 cm. The numbers of microphones per circle are chosen such that the microphone spacing in the circumferential direction is approximately the same as in the radial direction. There is a gradual increase of microphone density toward the center. The pattern is shown inside a gray square, representing an aluminum plate holding the array, in Fig. 9. The optimized side-lobe level was found to be $-8 \sim -9$ dB at the upper end of the frequency range ($5 \sim 50$ kHz), based on simulation of the near-field array pattern

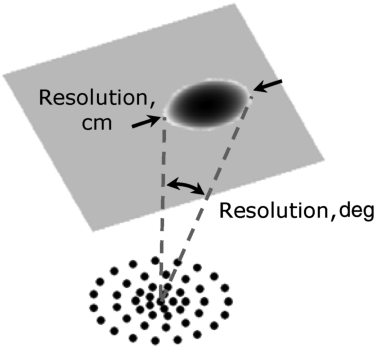

Fig. 10 Schematic diagram showing the definitions used for linear and angular resolution of arrays. Concentric black circles symbolize the high-frequency array. The gray plane indicates a scanning grid, parallel to the array plane. The distance between the two is 60 cm.

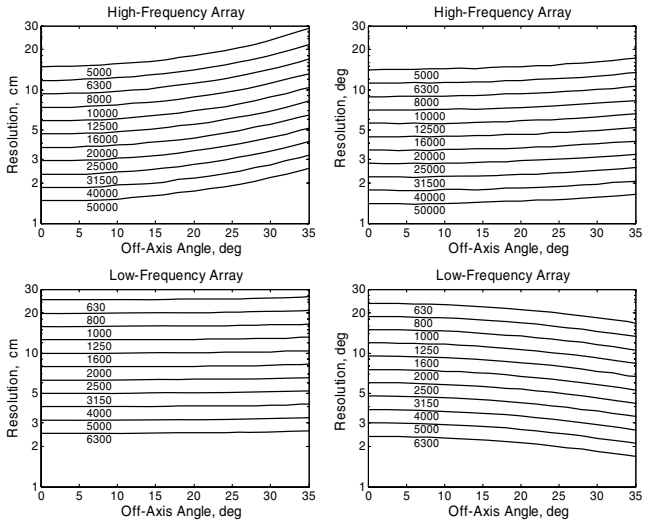

Fig. 11 Off-axis angle resolution of the low- and high-frequency arrays. The left-hand column shows linear resolution in centimeters and the right-hand angular resolution is in degrees. The frequency bandwidth is $\frac{1}{3}$ octave.

[8,19] for a monopole on-axis source at 60-cm distance. The solid angle formed by the high-frequency array and this typical source location is 0.132 sr (i.e., 2.1% of that of a hemisphere). Therefore, it is likely that beam-forming estimates the level of the source accurately in the direction of the array.

When an acoustic source is compact and located near the array axis, the on-axis resolution presented in the previous paragraph is sufficient to characterize the resolving capability of the array. However, when sources are significantly distributed, the off-axis resolution is a more useful measure of array performance. The off-axis resolution may be represented by two definitions, either linear or angular. Their definitions are shown schematically in Fig. 10, and their values are plotted as a function of the off-axis angle in Fig. 11. Note that the resolution deteriorates away from the axis, due to reduction of the effective array aperture.

Unlike the high-frequency array, the low-frequency array was mainly restricted by the size and structure of the wind tunnel itself. To obtain the best possible streamwise resolution, microphones were located on an elliptical pattern of approximate size 1.8×0.9 m. Because of the presence of a turntable supporting unit underneath the working section floor, it was found that some microphones could not be placed in optimally designed locations. Hence, a slight modification of their positions was inevitable. However, the simulation of a near-field array pattern showed that this would not have a detrimental effect, because of its low-frequency application. The actual array geometry and the ellipse of the optimum design are shown in Fig. 9. The streamwise resolution at a given frequency (down to around 650 Hz) is approximately half of the corresponding acoustic wavelength. The side-lobe levels in the upper frequency range (to around 6500 Hz) are similar to those of the high-frequency array. The resolution and side-lobe level quoted here are again related to an on-axis monopole at a 60-cm distance. In addition, the off-axis resolution is evaluated in Fig. 11. Because of the elliptical shape, the resolution of the low-frequency array is different for streamwise and spanwise directions; only the former is presented. Unlike the high-frequency array, the linear off-axis resolution is almost uniform due to the larger aperture, and the angular off-axis resolution thus decreases as the off-axis angle increases. The solid angle formed by the low-frequency array and a source 60 cm away on-axis is 2.11 sr, which is 33.6% of that of a hemisphere. Therefore, estimation of absolute source levels will be difficult for highly directional radiators. However, the array is still capable of detecting source locations across a wide spatial range and of estimating level differences between several test-model configurations, provided that the source directivity remains unchanged.

To reduce the installation cost and to increase the efficiency of measurements, the two arrays were designed to sit together on the tunnel floor. A similar type of a dual-array structure has been demonstrated previously [8]. Microphone signals from one or the other array were switched to the acquisition system, depending on the desired frequency range. Six channels from the arrays were made to coincide by moving their locations in the low-frequency array slightly to match their counterparts in the high-frequency array, because there is not enough space to accommodate additional microphones in the densely populated area close to the array centers. Such shifts were found not to have a noticeable effect on array simulations at the frequencies of interest, in which they are small on a wavelength scale. The six shared microphones are indicated by gray circles inside the gray square in Fig. 9.

V. Effect of Averaging on the Cross Spectra

After the arrays were installed, the background-noise characteristics of the wind tunnel could be further elucidated by the simultaneous use of increased numbers of microphones. In this section, we will focus on the cross spectra of the microphone pairs available in the arrays. Of interest is the extent to which they can be reduced by averaging. At low frequencies, this is limited by the well-correlated fan tones and (for pairs in close proximity) the partially coherent boundary-layer pressure fluctuations. Potential reductions at higher frequencies, however, have yet to be established. Here, they are investigated by considering the mean amplitude of the 1128 cross spectra available from each array. It is noted that the *mean* amplitude is evaluated by *spatially averaging* levels of all possible channel pairs, whereas the *average* mainly discussed in this section is done by averaging data blocks during FFT calculation.

Data were collected in the empty tunnel for 60 s. Then portions were extracted to form partial data sets of 30, 15, 7.5, and 3.75 s, down to a single block length (i.e., no averaging). The FFT block size was 1024, which, with 50% overlap, yields about 14,000 averages for the full duration set. Figure 12 shows the mean cross-spectrum amplitudes obtained for the high-frequency array at tunnel speeds of 20 m/s (Fig. 12a) and 40 m/s (Fig. 12b). The black lines bounding the results are the mean autospectra, which exhibit no significant variation with different numbers of averages. Pairs of black arrows in the plots show the effective resolution of the 16-bit data-acquisition system. Although the ideal dynamic range of a 16-bit machine is approximately 96 dB, it is usually limited to $70 \sim 80$ dB, depending on the precision of the system. In Fig. 12a, the mean spectrum level is shown to increase after a minimum at around 18 kHz, which is indicative of the noise floor of the measurement system. Thus, the spectrum beyond 18 kHz is unlikely to be meaningful. In the faster flow regime of Fig. 12b, more energy is present in the high-frequency region, and so such frequencies are now within the dynamic range of the acquisition system. Nonetheless, the empty tunnel spectra at 40 m/s reach the noise floor at around 30 kHz.

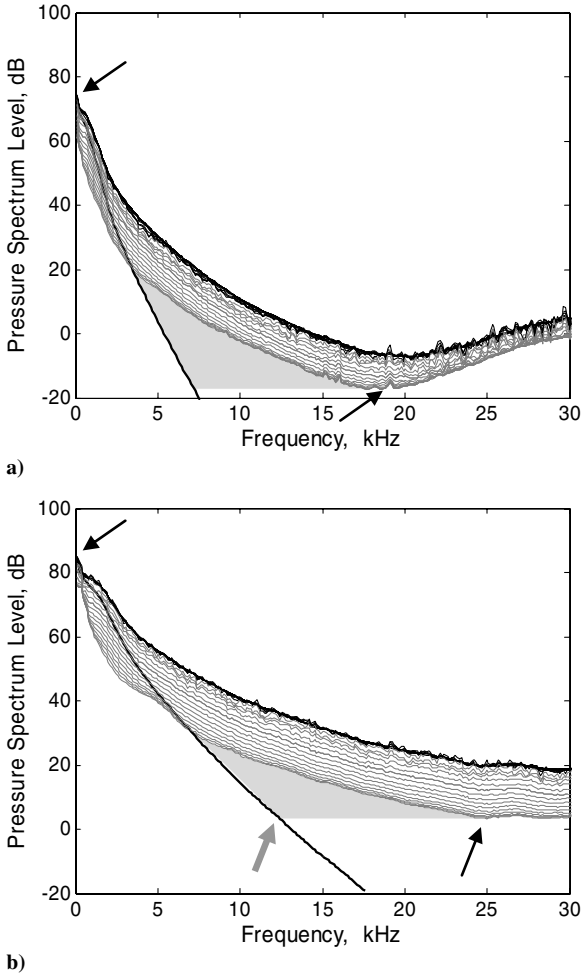

Fig. 12 The effect of number of averaging for the background-noise level of the wind tunnel. The amplitudes are the mean values over 48 microphones at the high-frequency array. The black lines on top of the spectra are mean autospectra, and a pile of gray lines are mean cross spectra showing different number of averages: a) 20 m/s and b) 40 m/s of tunnel speed. The frequency bandwidth is 117.2 Hz for both plots. The bottom edge of the three-edge gray areas represents the noise floor of the data-acquisition system. The thick single black line representing the left edge of the gray area is drawn by the Corcos model for the closest microphone pair.

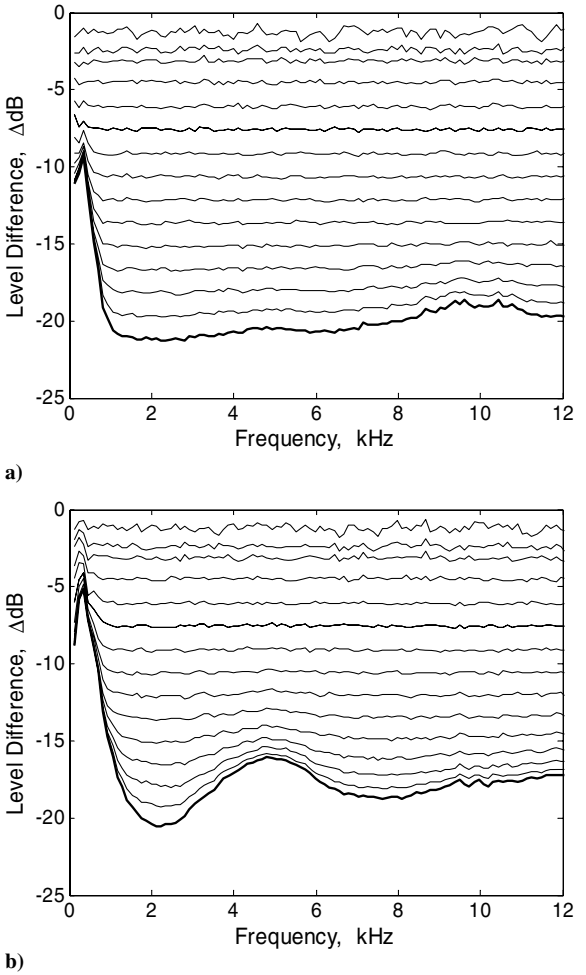

Fig. 13 Level difference of spatially averaged mean cross spectra between different number of averaging: a) mean cross spectra over all possible combination of pairs by 48 microphones at the low-frequency array and b) mean cross spectra at the high-frequency array.

The influence of the number of averages is better illustrated by the level-difference plots in Fig. 13. These show the difference between the mean autospectrum and cross spectrum for each partial data set. The level of 0 dB indicates that of the autospectrum at a given frequency. Figure 13a gives the results for microphone pairs in the low-frequency array, and Fig. 13b gives results for pairs in the high-frequency array. The number of averages approximately doubles between adjacent lines, apart from the top three, which show the results for one-, two- and three-block sets. At the lower frequencies, the presence of correlated components in the background noise is evident by the convergence of the curves. Note also that the levels for microphone pairs in the low-frequency array are lower than for the high-frequency array, because the microphone spacings are generally greater, and hence the noise signals are less correlated. Above 2 kHz, however, every doubling of the number of averages reduces the cross-spectral level by about 1.5 dB. The amount of reduction is similar between both arrays down to the level difference of −15 dB, but discrepancy is noticed afterward, depending on frequencies. Especially, the cross spectra of the high-frequency array seem to experience modulation associated with microphone spacings.

Finally, we consider how far the mean cross spectrum could be reduced, provided that we had enough data. The answer is illustrated by the three-edge gray areas in Fig. 12, under the assumption that there is no correlated background noise other than the noise floor of the acquisition system at high frequencies (represented by the bottom edge of the gray area) and the correlated turbulent boundary-layer pressures (for the closest microphone pair) at low frequencies, for which the Corcos model is denoted by the left edge. However, one would require about four hours of raw data to reach this level at the frequency indicated by the thicker gray arrow in Fig. 12b. The evaluation is based on −1.5 dB per doubling of average, which is observed mostly throughout the low-frequency array pairs in Fig. 13a. Because the high-frequency array pairs do not show the rate of −1.5 dB close to the thicker line in Fig. 13b, it would take a much longer time to achieve the gray arrow point. The influence of mean cross-spectrum level on source measurability is discussed in Sec. VI.C.

VI. Array Measurement and Beam Forming

The high-frequency array is usually run at a sampling rate of 120 kHz and the low-frequency array is run at 30 kHz, producing approximate analog bandwidths of 50 and 12 kHz, respectively. The measured signals in the time domain are transformed to complex pressures in the frequency domain by FFT. The matrix of cross spectra between all channel combinations is then formulated. As is routine for beam forming in wind tunnels [2,13,20], the diagonal elements of the matrix (i.e., the autospectra) are not included, due to the high background-noise level. Of the several methods available for beam forming, "conventional beam forming" was primarily used [20]. It is the frequency-domain counterpart of least-squares beam forming in the time domain. First, the scan grid containing the test model is defined. Source strength at each point is estimated by

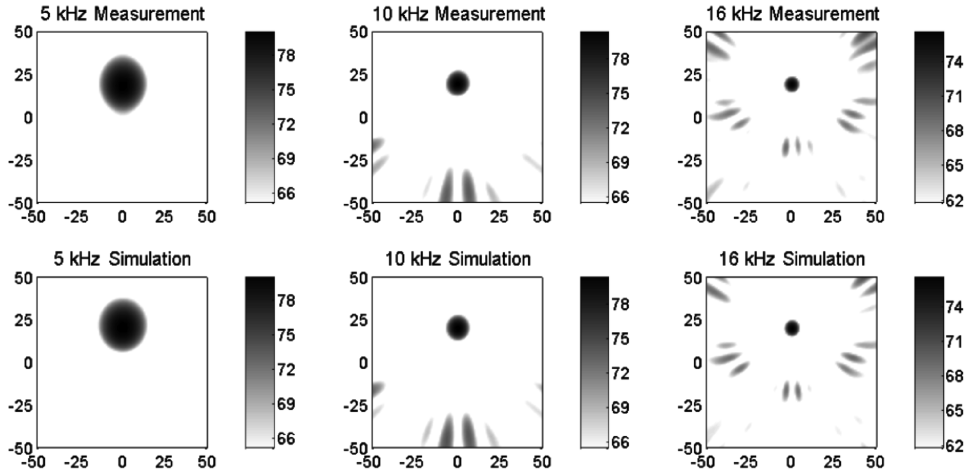

Fig. 14 Beam-forming source image maps for the measurement of a loudspeaker and the simulation of an ideal point source, conducted by the high-frequency array. The bandwidth is $\frac{1}{3}$-octave band. The grayscale is in decibel units. The dynamic range of images is 15 dB. The spatial dimensions are in centimeters.

finding the value that gives the best match between measured cross spectra and the field of a monopole located at that grid point. Beam forming is then capable of identifying the direction or location of the model source differently from that of background-noise sources, provided that the resolution of the array at a given frequency is fine enough to separate them. Finally, the output is displayed as image maps of the grid for a range of frequency bands.

In the following subsections, beam-forming results are presented for some shakedown measurements. They are categorized as either no-flow or with-flow measurements. The reason for conducting no-flow tests is that the quantification of the array performance is straightforward, because it is easy to control the source location.

A. No-Flow Loudspeaker Localization

First, a loudspeaker is placed in the quiescent wind tunnel to test the array's localization capability when there is no significant background noise. The operating range of the loudspeaker was from 1 to 20 kHz (in terms of $\pm$5-dB variation in its frequency response). The loudspeaker was placed at $x = 0$ and $y = 25$ cm from the array center at a height of 60 cm. It was oriented to face the array center to minimize directivity variations. The comparison between measurement and prediction was conducted in three steps. First, routine beam forming was conducted to obtain the source image maps, three of which (from the high-frequency array) are shown in the first row in Fig. 14. Next, the source strength in a given frequency band was estimated by integrating the beam-forming image and comparing the summed output with that generated by a reference case that has an ideal point source at the center of the scanning grid [20]. (Thus, for the estimation process, the scanning grid was chosen so that the center of the grid matched the location of the loudspeaker.) Finally, the frequency-dependent estimated source strength was used to simulate the beam-forming results for an ideal point source with uniform directivity at the location of the loudspeaker. The simulation images are shown in the bottom row in Fig. 14. It is clear that they closely match the experimental results. Figure 15 shows the mean square difference between the grid values, normalized by the mean square of the measured set. The bigger errors in the higher-frequency region may be attributed to the loudspeaker departing from point source behavior and the presence of excessive side lobes.

B. Diffraction of Sound Under the No-Flow Condition

A second no-flow test was devised to test the ability of the array to identify spatially distributed sources. The diffraction of sound around a circular disk was investigated theoretically and experimentally as early as 1947 [21], and the phenomenon is well understood. To realize it, first a compression driver was extended with a pipe to emulate a monopole point source (at frequencies for which the wavelength is much bigger than the diameter of the pipe)

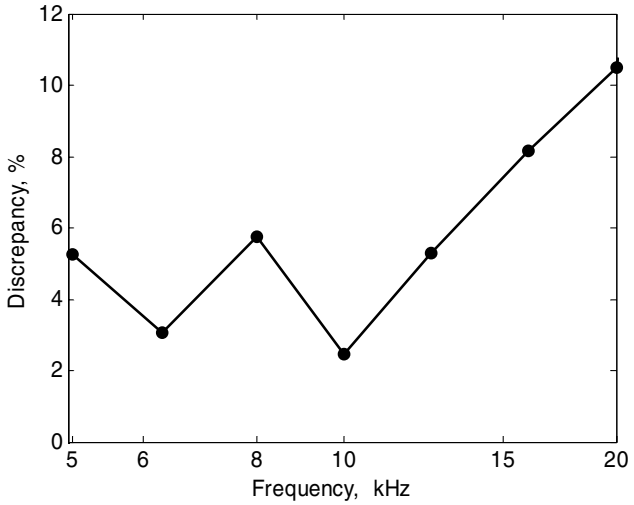

Fig. 15 Discrepancy in the beam-forming results between the measurement of a loudspeaker and the simulation of an ideal point source, conducted by the high-frequency array. The bandwidth is $\frac{1}{3}$-octave band.

and installed inside the quiescent wind tunnel. A 12-mm-thick plywood disk with a diameter of 71 cm was mounted under the pipe exit, as shown in Fig. 16. The distance between the disk and the pipe exit was 14.5 cm. The measurements and subsequent beam forming confirmed sound diffraction around the disk circumference, as seen in Fig. 17a, which shows that the edges of a disk act as secondary sources due to diffraction. The level of the grayscale bar is expressed as the level difference in ΔdB, where 0 dB corresponds to the acoustic pressure due to the driver alone. (Note, however, that the array was focused at the disk height for the beam forming.) The attenuation of the diffracted sound can thus be easily identified. Apart from the diffraction, the array system was also able to detect auxiliary aspects such as the sound leakage from the throat of the compression driver (Fig. 17a). It thus served as a useful tool to diagnose which components needed attention to improve the quality of the measurement. Driver leakage was evident at higher frequencies once a disk was introduced or the main source at the pipe exit was shielded. The same measurement was subsequently conducted in an anechoic chamber. However, a longer pipe was used to minimize contamination by a driver leakage. The disk was also placed further down, at 25 cm from the pipe exit, to reduce the ratio of diffraction path to transmission path compared with the ratio at the wind tunnel. The second test also captured the diffraction, as shown in Fig. 17b. The isolated spot near the center in Fig. 17b is regarded as being due

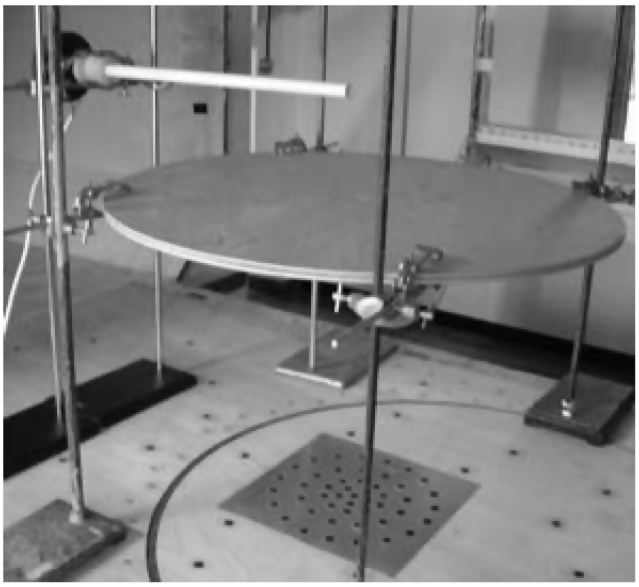

Fig. 16 Photo showing the measurement setup for sound diffraction around a disk in the Markham wind tunnel.

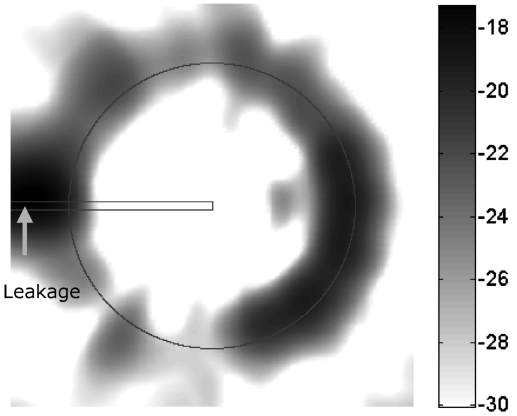

a)

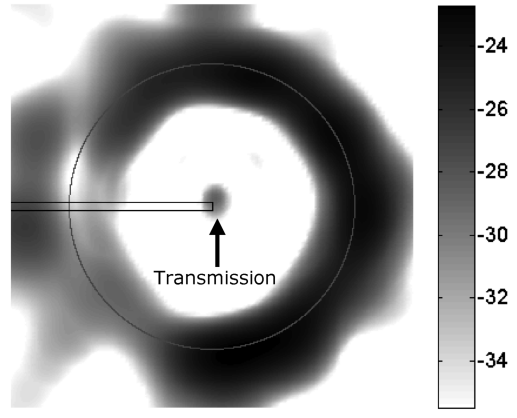

b)

Fig. 17 Beam-forming image plot of the high-frequency array showing the diffraction of sound from a pipe with diameter 2 cm (rectangle) around a disk with a diameter of 71 cm (circle): a) measurement in the Markham wind tunnel without flow and b) measurement in an anechoic chamber. The frequency is 6300 Hz at the $\frac{1}{3}$-octave band. The dynamic range of the plots is 13 dB. The level of 0 dB corresponds to the value obtained without a disk and with the beam-forming focus unchanged.

to transmission through the disk, rather than a side lobe. The side-lobe level at the frequency of 6.3 kHz may be estimated from Fig. 14, in which a 5-kHz beam-forming result is shown for the high-frequency array. There is no obvious side lobe present. (Note that the dynamic range of Fig. 14 is 2 dB more than that of Fig. 17 and the scanning grids are the same size in each case.) In both measurements, great care was taken to make sure that the pipe exit, disk center, and array center were aligned. Otherwise, a symmetrical diffraction pattern might not be observed.

C. Simulation on the Minimum Measurable Source Level

The background noise present in a closed-section wind tunnel places a limit on the measurable acoustic source level. To estimate this threshold, it is necessary to know the minimum achievable background-noise level. In Sec. V, it was shown that this level is dependent on the data-averaging scheme. Therefore, the data-acquisition and signal-processing parameters need to be specified first. We chose a reference scenario of 60-s data acquisition with FFT block sizes of 256 for the low-frequency array data sampled at 30 kHz and 1024 for the high-frequency array signals sampled at 120 kHz. This amounts in each case to around 14,000 averages with 50% overlap in the postprocessing and corresponds to the lowest lines in Figs. 12 and 13.

Given the difficulty of implementing a source with a known level in an operating wind tunnel, we have employed a hybrid scheme using the *measured* tunnel background noise and a *simulated* ideal source with a known strength, located 60 cm above the array center. The signal-to-noise ratio (SNR) of the ideal source was varied from 0 dB down to −12 dB in 3-dB steps, in which 0 dB indicates that the sound level of the source at the array center is equal to the spatially averaged mean level of all possible pairs of background cross spectra in each array.

Beam-forming image plots for various signal-to-noise ratios are shown with a noise-free case in Fig. 18 for both arrays. The measured tunnel speed is 40 m/s. The displayed $\frac{1}{3}$-octave band center frequencies are 4 and 16 kHz for the low- and high-frequency arrays, respectively. For these frequencies, the streamwise on-axis resolution of the low-frequency array is similar to the on-axis resolution of the high-frequency array. The dynamic range of the images is 13 dB. The absolute levels shown in the grayscale bar are reduced according to the SNR. The source strength for the displayed noise-free simulation is chosen to be the same as that for a SNR of 0 dB. It is observed that for the given dynamic range, source detection is straightforwardly possible down to a SNR of −6 dB and may well be feasible at a SNR of −9 dB with some prior knowledge of the source location. Simulation for other frequencies with the SNR of −6 dB is shown in Fig. 19 for the low-frequency array.

D. With-Flow NACA-0012 Model Measurement

One of the first inflow measurements for the array system was to detect an aeolian tone from a thin cylinder. This was useful because the flow-induced frequency is known and varies with the flow speed. Then the arrays were employed to measure the vortex-shedding tonal noise [22,23] generated by a NACA-0012 wing model with a chord of 15 cm and a trailing-edge thickness of 0.7 mm. Its boundary layer was later tripped by a wire of 0.55-mm diameter placed at the location of the maximum thickness at the wing. The angle of attack of the wing was zero. Figure 20 shows the magnitude of the cross spectra measured for both untripped and tripped boundary layers. The microphone pair is at the center of the high-frequency array with streamwise spacing 2.3 cm. The freestream tunnel speeds were 20, 30, and 40 m/s, corresponding to chord-based Reynolds numbers of 207,000, 310,000, and 414,000, respectively. The untripped boundary-layer cases, denoted by solid lines, show distinct harmonic tones generated by vortex shedding at the trailing edge. Subsequent boundary-layer tripping, indicated by dashed lines, was demonstrated to be effective in suppressing those tones, in agreement with previous work [23]. Tonal noise is thought to radiate from a wing when the laminar boundary layer extends to its trailing edge [22], and hence forced early transition to a turbulent boundary

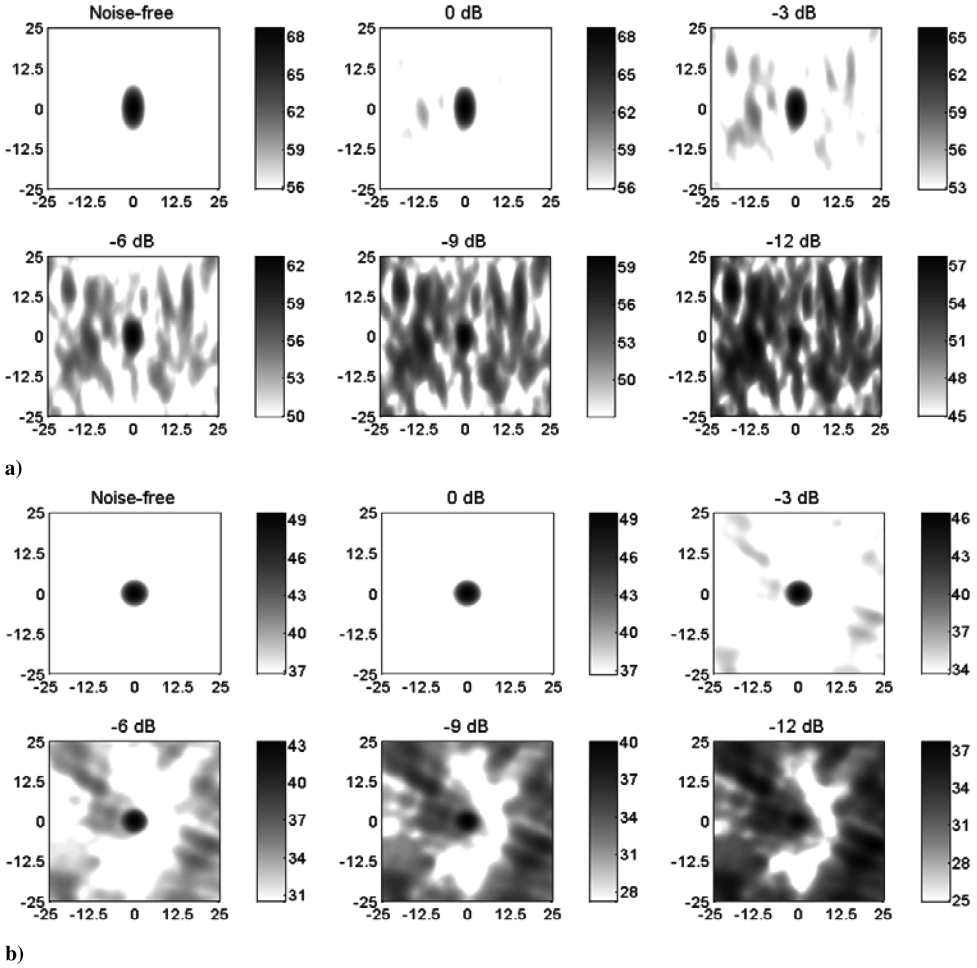

Fig. 18 Beam-forming image plot of simulations indicating the minimum measurable source level: a) the low-frequency array at 4 kHz and b) the high-frequency array at 16 kHz at $\frac{1}{3}$-octave band. The title for each plot shows the signal-to-noise ratio with the noise level being the mean cross spectra based on all possible combination of each array of microphone pairs. The tunnel speed is 40 m/s, which flows from left to right in the image. The dynamic range of the image is 13 dB. The spatial dimension is expressed in centimeters and its origin corresponds to the center of the array. The height of the simulated point source is 60 cm.

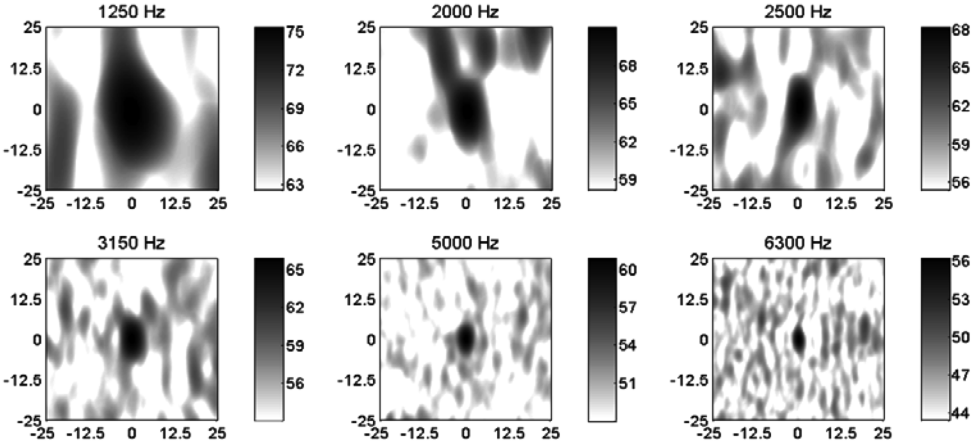

Fig. 19 Beam-forming image plot of simulations indicating the minimum measurable source level for the low-frequency array at the SNR of −6 dB. The frequency is at $\frac{1}{3}$-octave band. The tunnel speed is 40 m/s, which flows from left to right in the image. The dynamic range of the image is 13 dB. The spatial dimension is expressed in centimeters and its origin corresponds to the center of the array. The height of the simulated point source is 60 cm.

layer is expected to reduce its level, such as tripping or increasing Reynolds number with higher flow speed. The base cross-spectral lines in Fig. 20 are indicating the wind-tunnel background noise rather than broadband trailing-edge noise of the wing model. As drawn in Sec. V, the level of these base levels is dependent on the data-analysis scheme. The current output is for the 60-s-long data sampled at 120 kHz with the average of about 3500 with 50% overlap, which yields the constant bandwidth of 29.3 Hz.

The beam-forming calculation was carried out for both boundary-layer cases. Both low- and high-frequency arrays were employed to see how the same event is interpreted by each. The result chosen for presentation here is for a wind speed of 30 m/s and a frequency of

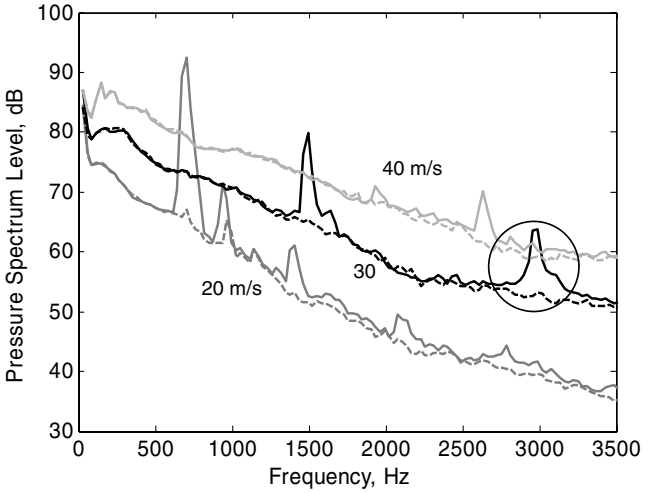

Fig. 20 Cross-spectrum measurements of a NACA-0012 scaled-wing model with untripped (solid lines) and tripped (dashed lines) boundary layer. The microphone pair is placed 2.3 cm apart along the streamwise axis. Bandwidth is 29.3 Hz with 3500 averages.

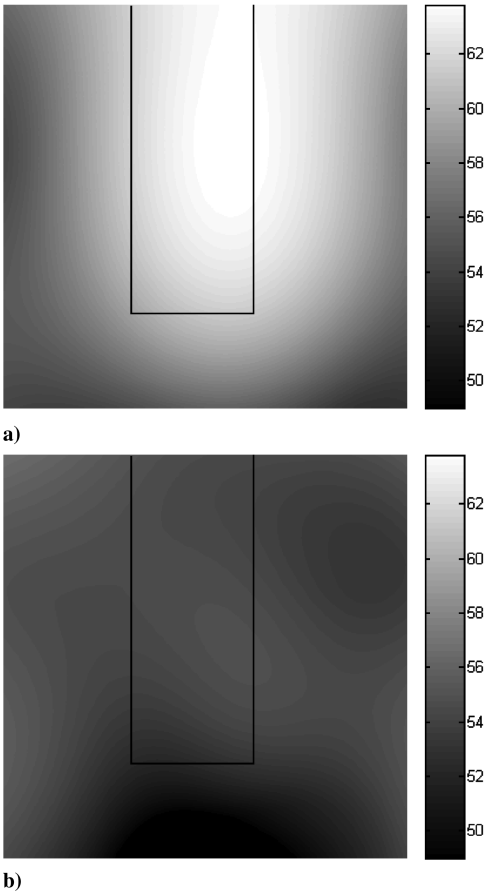

a)

b)

Fig. 21 Beam-forming source image plot of the high-frequency array: a) tonal noise generated by a NACA-0012 wing model and b) the case with boundary-layer tripping. The wind blows at 30 m/s from left to right. The frequency is 3150 Hz at $\frac{1}{3}$-octave band. The geometry of the wing with a chord of 15 cm is indicated by the black line. The dynamic range of the plots is 15 dB.

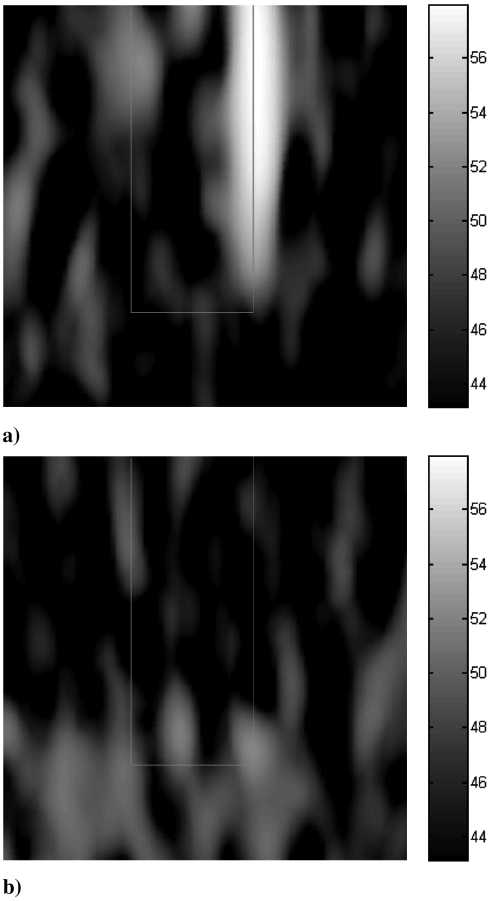

a)

b)

Fig. 22 Beam-forming source image plot of the low-frequency array: a) tonal noise generated by a NACA-0012 wing model and b) the case with boundary-layer tripping. The wind blows at 30 m/s from left to right. The frequency is 3150 Hz at $\frac{1}{3}$-octave band. The geometry of the wing with a chord of 15 cm is indicated by gray lines. The absolute sound level is not matched to that in Fig. 21.

3150 Hz at $\frac{1}{3}$-octave band, which corresponds to the second harmonic of tonal noise, marked by a circle in Fig. 20. The frequency chosen belongs to the higher-frequency region of our low-frequency array and is slightly below the lower-end frequency of our high-frequency array. For this particular application, the built-in high-pass filter at 5 kHz was therefore not used for the high-frequency array data acquisition. Because the noise level for 30 m/s is not severe, most of the frequency range can be acquired with the 16-bit data logger without losing meaningful information. Figure 21a shows how the vortex-shedding tone of the untripped wing along its trailing edge appears to the high-frequency array. In Fig. 21b, the boundary-layer tripping subdues the tone by a significant amount. Figure 22a demonstrates that the low-frequency array can produce a finer image of the tones than its high-frequency counterpart. But it is also clear the results show extraneous images caused by either flow noise or the side lobes. In Fig. 22b, the tonal noise is again seen to be dramatically suppressed by boundary-layer tripping. Remaining relatively bright spots represent how background noise is seen by the array. Because the two arrays are installed and run together in the Markham wind tunnel, they can complement each other, especially in an overlapped frequency range between the two.[††] This could help alleviate a potential need to design and manufacture a new array optimized for such a transitional frequency range.

In Sec. V, the dependence of the cross-spectral background noise on the number of averages was discussed. In this respect, beam-forming images based on less-averaged processing are a useful comparison with Fig. 22a. The data used for Fig. 22 were acquired for 60 s at a 30-kHz sampling rate. It was converted to the frequency domain with an FFT block size of 256, yielding a bandwidth of 117.2 Hz. (Note that these are different from the parameters for

[††]For beam-forming images, the absolute levels of source strengths are not compared for the low- and high-frequency arrays. That is because of frequency dependence of beam-forming resolution and distributed noise sources along the trailing-edge.

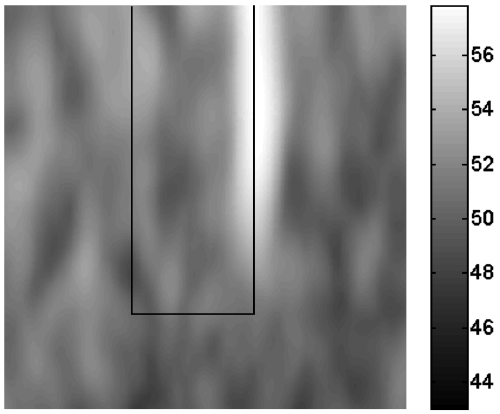

a)

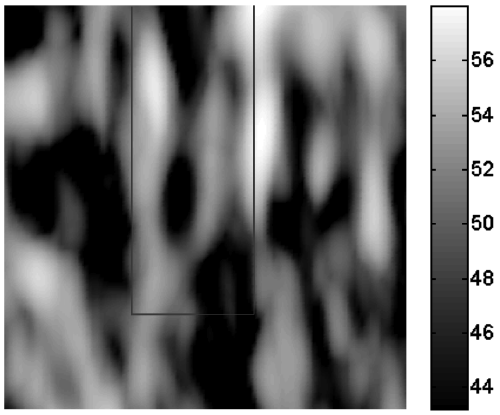

b)

Fig. 23 Effect of the averaging number on the beam forming of the untripped NACA-0012 model by the low-frequency array (originally shown in Fig. 22a, which is based on FFT block size of 256 for 60-s-long data): a) FFT block size of 4096 for 60-s data and b) FFT block size of 256 for 3.75-s data. Both cases have 16 times less averaging than that of Fig. 22a. The wind blows at 30 m/s from left to right. The frequency is 3150 Hz at $\frac{1}{3}$-octave band. The geometry of the wing with a chord of 15 cm is indicated by gray lines.

Fig. 20.) Then the narrowband results were combined to produce the image based on the $\frac{1}{3}$-octave band. These data were first processed again with an increased FFT block size of 4096 and thus 16 times fewer averages. The corresponding beam-forming image is shown in Fig. 23a. Then the original FFT block size of 256 was used with a 16th of the original data set (see Fig. 23b). It is apparent that the performance of the reduced-averaging analyses is not as good as the reference case in detecting the vortex-shedding tones, because the apparent background-noise level is higher.

VII. Conclusions

This paper described a range of practical issues associated with the implementation of phased microphone arrays in a closed-section aerodynamic wind tunnel. During a feasibility study, microphones with protection grids were found to generate excess flow-induced noise levels as high as 20 dB at a tunnel speed of 60 m/s. Hence, microphones with exposed diaphragms of smaller size were chosen for the array system. Sources and levels of background noise in the empty tunnel were also investigated. Turbulent boundary-layer pressure fluctuations were identified by their cross-spectral phase signature. However, it was shown that there is no benefit in recessing microphones with an acoustically transparent cover, compared with flush mounting. Therefore, two flush-mounted arrays were implemented: the larger for $650 \sim 6500$ Hz and the smaller for $5 \sim 50$ kHz. The cross-spectral characteristics of array microphone pairs were further studied in relation to the minimum measurable source level. It was shown that a source as quiet as 6 dB below the mean cross-spectral level of background noise could be detectable. It was also demonstrated that for a given tunnel operating condition, cross-spectral levels depend on the number of averages, which thereby determines the quality of beam-forming output images and hence the detectability of a source.

Acknowledgments

The work was carried out within the Silent Aircraft Initiative, funded by the Cambridge–MIT Institute. The authors would like to acknowledge the general contribution of all members of the Silent Aircraft Initiative and to especially thank John Clark in the Department of Engineering's Aerodynamics Laboratory for manufacturing the phased microphone arrays and for his assistance in operating the Markham wind tunnel.

References

[1] Duell, E., Walter, J., Arnette, S., and Yen, J., "Recent Advances in Large-Scale Aeroacoustic Wind Tunnels," 8th AIAA/CEAS Aeroacoustics Conference and Exhibit, Breckenridge, CO, AIAA Paper 2002-2503, 2002.

[2] Mosher, M., "Phased Arrays for Aeroacoustic Testing: Theorectical Development," 2nd AIAA/CEAS Aeroacoustics Conference, State College, PA, AIAA Paper 96-1713, 1996.

[3] Sijtsma, P., and Holthusen, H., "Source Location by Phased Array Measurements in Closed Wind Tunnel Test Sections," 5th AIAA/CEAS Aeroacoustics Conference and Exhibit, Bellevue, WA, Vol. 1, AIAA Paper 1999-1814, 1999.

[4] Brooks, T. F., and Humphreys, W. M. J., "Effect of Directional Array Size on the Measurement of Airframe Noise Components," 5th AIAA/CEAS Aeroacoustics Conference and Exhibit, Bellevue, WA, AIAA Paper 1999-1958, 1999.

[5] Jaeger, S. M., Horne, W. C., and Allen, C. S., "Effect of Surface Treatment on Array Microphone Self-Noise," 6th AIAA/CEAS, Aeroacoustics Conference and Exhibit, Lahaina, HI, AIAA Paper 2000-1937, 2000.

[6] Holthusen, H., and Smit, H., "A New Data Acquisition System for Microphone Array Measurements in Wind Tunnels," 7th AIAA/CEAS Aeroacoustics Conference and Exhibit, Maastricht, The Netherlands, AIAA Paper 2001-2169, 2001.

[7] Oerlemans, S., and Sijtsma, P., "Determination of Absolute Levels from Phased Array Measurements Using Spatial Source Coherence," 8th AIAA/CEAS Aeroacoustics Conference and Exhibit, Breckenridge, CO, AIAA Paper 2002-2464, 2002.

[8] Underbrink, J. R., "Aeroacoustic Phased Array Testing in Low Speed Wind Tunnels," *Aeroacoustic Measurements*, edited by T. J. Muelller, Springer–Verlag, Heidelberg, Germany, 2002, pp. 98–217.

[9] Guo, Y. P., Yamamoto, K. J., and Stoker, R. W., "Component-Based Empirical Model for High-Lift System Noise Prediction," *Journal of Aircraft*, Vol. 40, No. 5, 2003, pp. 914–922.

[10] Horne, W., James, K., Arledge, T., Soderman, P., Burnside, N., and Jaeger, S., "Measurements of 26%-Scale 777 Airframe Noise in the NASA Ames 40- by 80 Foot Wind Tunnel," 11th AIAA/CEAS Aeroacoustics Conference, Monterey, CA, AIAA Paper 2005-2810, 2005.

[11] Dowling, A. P., and Ffowcs Williams, J. E., *Sound and Sources of Sound*, Ellis Horwood, Chichester, England, U.K., 1983.

[12] *Acoustical Terminology*, American National Standards Inst., Rept. ANSI S1.1-1994 (R2004), New York, 1994.

[13] Dougherty, R. P., "Beamforming in Acoustic Testing," *Aeroacoustic Measurements*, edited by T. J. Muelller, Springer–Verlag, Heidelberg, Germany, 2002, pp. 62–97.

[14] Hamid, H., and Horne, C., "An Experimental Study of the Response of a Condenser Microphone Installed in a Flat Plate," 35th Aerospace Sciences Meeting and Exhibt, Reno, NV, AIAA Paper 1997-491, 1997.

[15] Corcos, G. M., "The Structure of the Turbulent Pressure Field in Boundary-Layer Flows," *Journal of Fluid Mechanics*, Vol. 18, No. 3, 1964, pp. 353–378. doi:10.1017/S002211206400026X

[16] Blake, W. K., *Mechanics of Flow-Induced Sound and Vibration, Volume 2: Complex Flow–Structure Interactions*, Academic Press, New York, 1986.

[17] Guo, Y. P., and Joshi, M. C., "Noise Characteristics of Aircraft High Lift Systems," *AIAA Journal*, Vol. 41, No. 7, 2003, pp. 1247–1256.

[18] Munro, S. E., Ahuja, K. K., and Englar, R. J., "Noise Reduction Through Circulation Control," 39th Aerospace Sciences Meeting and Exhibit, Reno, NV, AIAA Paper 2001-0666, 2001.

[19] Johnson, D. H., and Dudgeon, D. E., *Array Signal Processing: Concepts and Techniques*, Prentice–Hall, London, 1993.

[20] Sijtsma, P., "Experimental Techniques for Identification and Characterisation of Noise Sources," *Advances in Aeroacoustics and Applications*, VKI Lecture Series 2004-05, Vol. 1, edited by J. Anthoine and Hirschberg, A., Von Karman Inst. for Fluid Dynamics, Rhode-Saint-Genèse, Belgium, 2004.

[21] Primakoff, H., Klein, M. J., Keller, J. B., and Carstensen, E. L., "Diffraction of Sound Around a Circular Disk," *Journal of the Acoustical Society of America*, Vol. 19, 1947, pp. 132–142. doi:10.1121/1.1916410

[22] Paterson, R., Vogt, P., Fink, M., and Munch, C., "Vortex Noise of Isolated Airfoils," *Journal of Aircraft*, Vol. 10, No. 5, 1973, pp. 296–302.

[23] Longhouse, R. E., "Vortex Shedding Noise of Low Tip Speed, Axial Flow Fans," *Journal of Sound and Vibration*, Vol. 53, No. 1, 1977, pp. 25–46. doi:10.1016/0022-460X(77)90092-X

N. Chokani
Associate Editor